Composites Part B 145 (2018) 206–214

Contents lists available at ScienceDirect

Composites Part B

journal homepage: www.elsevier.com/locate/compositesb

Effect of laser cleaning in Laser Assisted Joining of CFRP and PC sheets

S. Genna[a,d], F. Lambiase[b,d], C. Leone[c,d,*]

[a] Department of Enterprise Engineering, University of Rome Tor Vergata, Via del Politecnico 1, 00133, Rome, Italy
[b] Department of Industrial and Information Engineering and Economics, University of L'Aquila, via G. Gronchi 18, Zona Industriale di Pile, 67100, AQ, Italy
[c] Department of Engineering, University of Campania Luigi Vanvitelli, Via Roma 29, 81031, Aversa, Ce, Italy
[d] CIRTIBS Research Centre, University of Naples Federico II, P. le Tecchio 80, 80125, Naples, Italy

ARTICLE INFO

Keywords:
Polymers joining
Cleaning treatment
Laser welding
Composite
Hybrid structure

ABSTRACT

The present paper investigates the influence of laser cleaning of Carbon Fibre Reinforced Plastic (CFRP) surface when joining CFRP to Polycarbonate (PC) sheet by means of laser assisted Joining.

Experimental tests were conducted to perform polycarbonate-CFRP (with epoxy matrix) joints. The laser cleaning treatment was carried out on CFRP laminate adopting a 30 W Q-switched Yb:YAG fibre laser. Laser assisted joining was performed adopting a continuous wave 200 W diode laser. Untreated samples were adopted as reference. Morphological analysis and single lap shear tests were conducted to characterize the joints. Infrared thermography (IRT) was carried out to determine the temperature distribution and variation during the joining process. ANalysis Of VAriance was applied to investigate the effect of the process parameters, (laser power, energy, and treatment) on the extension of the bonded area and the mechanical properties. The results show that laser pre-treatment enables a significant increase of the joint strength which is, under the optimal conditions, more than double than the reference samples: However, considering the apparent shear strength, the laser pre-treatment does not produce a significant advantage, as it mainly resulted in the enlargement of the bonded area.

1. Introduction

The growing demand of light-weight structures, especially in transport, results in wider employment of hybrid structures made of different materials. In this context, the employment of multi-material assemblies represents a possible solution; coupling materials with different physical and mechanical behaviours can offer different opportunities. For example, in the case of Carbon Fibre Reinforced plastics CFRP coupled with polycarbonate (PC), it is possible to obtain hybrid structures, characterized by high strength and toughness, with the presence, if necessary, of transparent areas, for inspection or aesthetical reasons. On the other hand, as PC shows good impact resistance, it can be adopted either as matrix for Carbon Fibre Reinforced Thermoplastics (CFRTP), as adopted in Ref. [1], or as core between two thin plies of carbon cross textile fibre/epoxy (CFRP/PC/CFRP) [2].

The main concern of multi-material assemblies is the adoption of a suitable joining process. Mechanical joining processes (such as riveting or bolting) [2] are often adopted for this purpose. However, the stress concentration and the long working time, due to the drilling operations, represent great limitation to their application. In recent years, fast mechanical joining methods, which do not require pre-drilled holes, were developed, such as Self-Pierce Riveting (SPR) and Mechanical Clinching (MC). Owing to their simplicity, robustness, low cost, and high productivity, many studies were conducted to adapt these processes to hybrid metal–polymer [3,4] and metal–Fibre Reinforced Plastics (FRP) [5–8] joints. However, these processes still suffer some drawbacks; e.g. high stress concentration (due to the spot joints) and the requirement of access from both sides of the joint. In addition, when continuous fibres are adopted as reinforcement, delamination is present near the joint [7,9]. Finally, these processes can be employed only when the material placed on the punch side has high strength and shows certain plasticity.

Besides mechanical joining processes, adhesive bonding [10] and welding [11] are also widely used. Adhesive bonding enables good stress distribution, good fatigue life, corrosion resistance, and high strength-to-weight ratio as compared to mechanically fastened joints. In addition, it does not cause stress concentration or fibres interruption. Despite these advantages, adhesive bonding shows some drawbacks and special requirements, including: substrate preparation, long processing time (due to preparation of substrate and curing time), specialized workers and involves high environmental impact, due to emission of volatile organic compounds as well as the employment of solvents used for substrates preparation [12]. In addition, adhesive bonding introduces a third material (the adhesive) during the process [13] and

* Corresponding author. Department of Engineering, University of Campania Luigi Vanvitelli, Via Roma 29, 81031, Aversa, Ce, Italy.
E-mail address: claudio.leone@unicampania.it (C. Leone).

https://doi.org/10.1016/j.compositesb.2018.03.032
Received 17 November 2017; Received in revised form 20 February 2018; Accepted 16 March 2018
Available online 17 March 2018
1359-8368/ © 2018 Elsevier Ltd. All rights reserved.

bonding thermoplastic matrix composites requires special attention given the low chemical affinity of this matrix with the structural adhesives.

In order to overcome the aforementioned limitations, in last years, new joining processes, such as Friction Lap Welding (FLW), friction spot welding, and friction based stacking, were developed and studied. For example, FLW was adopted to joint metals to thermoplastics [14,15] or CFRP to aluminium [16,17]. Friction Assisted Joining was employed to join thermoplastic polymers [18,19], metals with thermoplastic polymers [20,21] and reinforced thermoplastic polymers [17,22–26]. Moreover, it was also adopted to joint metals with FRP with long fibres [22]. On the other hand, these processes enable obtaining joints with low quality finishing and they require very stiff clamping systems, due to high loads involved during the processes.

A valid alternative to the aforementioned joining processes are Laser Transmission Welding (LTW) and Laser-Assisted Joining (LAJ) [27] to weld thermoplastics and to join hybrid metal-plastic structures, respectively. During LTW and LAJ processes, the laser beam heats and melts the plastic component and promotes the adhesion (both mechanical and chemical). The substrates interface can be heated either by transmission of the radiation through the plastic, or by means of conduction throughout a heated metal. LAJ process is characterized by several advantages as compared to adhesive bonding, e.g. fast joining (no curing time), localized heating, no vibration, low residual stresses [28] and no employment of further components (i.e. the adhesive). During LTW and LAJ the parts need to be pressed together to reduce the gap and allow the adhesion [29]. However, fine calibration of the laser processing parameters (e.g. power, scanning speed, stand-off-distance, clamping pressure) is required. Indeed, previous studies indicate that these parameters influence the temperature distribution inside the bonded area [30], the residual stress [31], the presence of contact between the materials, the polymer crystallinity [32,33] and, hence, the bond quality and strength.

Recently, LTW was adopted to weld fibre-reinforced thermoplastics [34,35], like Glass Fibre Reinforced Polyamide (GFR-PA66) to PC, reaching a shear strength of 4 MPa [36]. To estimate the temperature distribution inside the bonded area and consequently to optimize the weld performance, LTW of composites requires accurate modelling of the interaction of the laser beam with semi-transparent composites [37]. However, when reinforced plastics are welded, high care should be paid to the fibres orientation. Indeed, carbon fibres have great thermal conductivity compared to the matrix material. Consequently, the heat is conducted along the fibres and the weld seam geometry is affected by the local orientation of the fibres [38].

So far, Laser Assisted Joining processes have been employed to weld thermoplastics [39–43], fibre reinforced thermoplastics [34–37] including CFRP composites [44–46] and different metals: PET-AISI304 [27], PET-titanium [47–51], PMMA-AISI304 [52,53], Polytetrafluoroethylene (PTFE)-titanium [54], PET-aluminium [55], ABS-zinc-coated steel [56], PC-AISI304 [57] as well as to join fibre-reinforced thermoplastics (PC, PA66, PE) [35,36,45].

In a previous paper [58], the LAJ of thermoplastics sheet and composite with thermosetting matrix was reported for the first time. In that work, the process was conducted without prior removing the layer of epoxy that covered the irradiated carbon fibres. Thus, the main mechanisms developed during the laser processing were determined: heating of the carbon fibres, vaporization of the covering layer of epoxy, heating the overlying thermoplastic material and adhesion between the fibres and the thermoplastic material. Different phenomena were involved in the process that limited the strength of the joints, including: production of fumes (of both the epoxy and polycarbonate materials since the high temperatures involved), thermal degradation of the polycarbonate with formation of entrapped fumes at the interface and bubbles, which reduced the effective adhesion area, degradation of the epoxy layer underlying the layer of exposed carbon fibres. These issues were found under all processing conditions. On the other hand, when low energies were adopted, poor epoxy was removed from the interface layer. This affected the joint strength as it reduced the adhesion area between the PC and the carbon fibres. Generally, in order to achieve the formation of the joint, the processing conditions should lead to the removal of the epoxy layer. To this end, a temperature of at least 400 °C should be reached. Such temperature is very close to that of degradation of the PC material (540 °C).

The present study deals, for the first time, on the effect of laser pre-treatment on the joint strength of PC sheet to CFRP laminate, obtained by Laser Assisted Joining. To this end, laser joining at different process conditions was performed on autoclave cured CFRP laminate and PC sheets, with and without a laser cleaning pre-treatment of the CFRP surface. The laser pre-treatment was carried out adopting a 30 W Q-switched Yb:YAG fiber laser; while the joints were performed adopting a 200 W diode laser.

After joints production, mechanical tests were carried out; ultimate tensile strength and apparent shear strength were measured. Moreover, fracture surfaces analysis was performed. Infrared thermography (IRT) was also performed in order to understand the interaction phenomena occurring during the laser joining. ANalysis Of VAriance was applied to study the influence of the process parameters (laser power, energy, and treatment), on the bonded area extension and the mechanical properties.

2. Materials and methods

2.1. Materials

Polycarbonate (PC) sheets, 2.0 mm in thickness, supplied by Bayer, were coupled to CFRP laminates with thickness of 1.5 mm. The CFRP laminate was manufactured by means of hot pressing for 2 h at 130 °C and 5 MPa, as suggested by the resin supplier. Plain weave (SK Chemicals, UGN200) carbon fibre prepegs (0/90°, 50% in the warp and weft directions, MRC Pyrofil, TR30S) and a thermosetting epoxy resin (bisphenol-A type epoxy + phenol novolac type epoxy) were used for the production of the CFRP laminate [7]. The thermal characteristics of the materials are summarized in Table 1.

2.2. CFRP laser cleaning

Laser cleaning pre-treatment of the CFRP laminate (removal of the covering epoxy layer) was performed by means of a 30 W Q-switched Yb:YAG fibre laser (YLP-RA 30-1-50-20-20 by IPG), working at the fundamental wavelength of 1064 nm. In this laser system, the laser beam is moved by two galvanometric mirrors, placed into the scanner head, and, then, focused by a “flat field lens” of 160 mm in focal length. Thus, the resulting beam spot diameter is about 80 μm. In Table 2 the laser system characteristics are summarized. In order to treat the entire surface to be joined, more parallel lines, spaced of fixed quantities (called hatch distance, Hd), were performed, according to the procedures described in Refs. [62–64] and the schematic shown in Fig. 1. During the cleaning treatment the following parameters were adopted: hatch distance of 40 μm, beam speed of 2000 mm/s, average power of 30 W, pulse frequency of 30 kHz and pulse duration of 50 ns. Under these conditions the pulse power resulted of 20 kW and the pulse energy of 1 mJ. These values were selected on the basis of previous experiences

Table 1
Characteristic temperatures of polycarbonate and epoxy resin.

Material	Glass Transition Temperature, Tg [°C]	Melting temperature, Tm [°C]	Degradation temperature, Td [°C]
PC	154 [59]	230	540 [60]
Epoxy	165	–	450 [61]

Table 2
Laser systems characteristics.

Characteristic	Symbol	Laser cleaning	Laser joining	Unit
Source	–	Yb:YAG	Diode	
Wavelength	λ	1064	975	nm
Nominal average power	Pa	30	200	W
Mode		PW	CW	-
Pulse frequency	F	30 ÷ 80	–	kHz
Pulse duration	D	50	–	ns
Maximum pulse power	Pp	20[a]	–	kW
Maximum pulse energy	Pe	1[a]	–	mJ
Maximum scan speed	Ss	5000	200	mm/s
Mode	TEM	00	multimode	–
	M^2	1.2 ÷ 1.5	n.a.	–
Focused spot diameter	–	80	6000	μm

[a] at P = 30 W and F = 30 kHz.

[62–64] and preliminary tests. Under these conditions, it was possible to remove the first matrix layer up to the fibres exposition, avoiding apparent damages, according to [63–65]. Fig. 2 shows the CFRP laminate surface in both the analysed conditions: "As Received" (AR) and "Laser Cleaned" (LC).

2.3. Laser assisted joining

A diode source (DLR-200-AC by IPG) with maximum power of 200 W was used to perform Laser-Assisted Joining process. A collimator was adopted to obtain a laser beam with circular shape of 6 mm in diameter. In Table 2 the laser system characteristics are summarized.

CFRP samples, 40 mm × 80 mm in plane dimensions, were placed in a clamping system, mounted in a 3 + 1 CNC axis machine, with maximum speed of 200 mm/s. The PC sheets were placed on the CFRP samples with an overlap of 40 mm. The sheets were clamped with a pressure of about 1 MPa; such a value was selected on the bases of preliminary tests. The laser beam was moved at the centre of the overlapping length area. In Fig. 3 a schematic of the Laser Assisted Joining setup is depicted. Note that the PC sheet was placed at the laser beam side (being almost transparent to the diode laser radiation [66]). The adopted setup enabled to produce joints similar to those suggested by ASTM D3163-01 standard. In Fig. 4 the sample geometry, with the dimensions, is shown. In the figure, the central area namely "Bonded Region" represents the irradiated area.

2.4. Experimental procedure

In order to investigate the effect of the surface treatment and the effect of the process parameters adopted in the LAJ process, a full factorial plan was developed and tested, according to the Design of Experiments (DOE) methodology. The levels of the experimental plan,

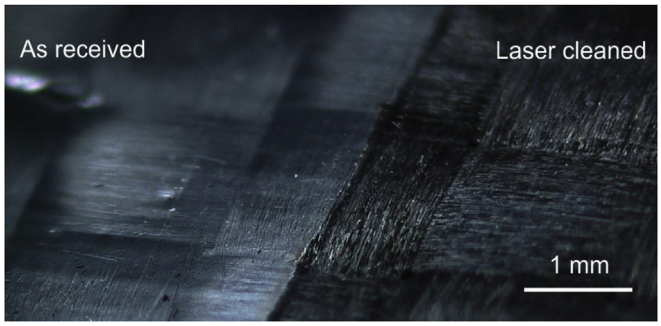


Fig. 2. Macrograph of the CFRP laminate surface in As Received (AR) and Laser Cleaned (LC) conditions.

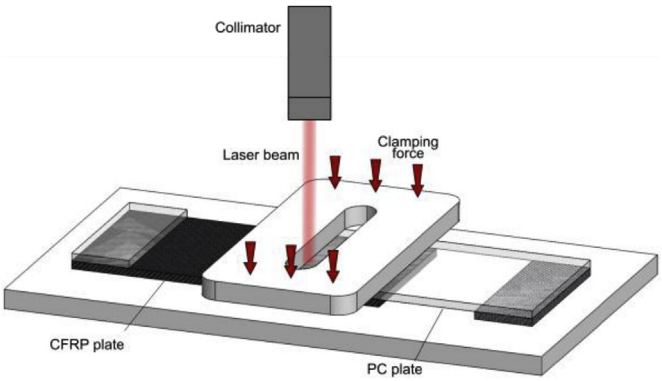


Fig. 3. Schematic representation of Laser Assisted Joining setup.

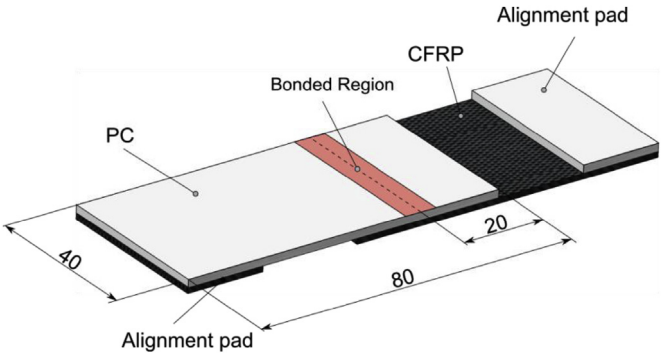


Fig. 4. Single lap joint geometry (ASTM D3163–01 standard).

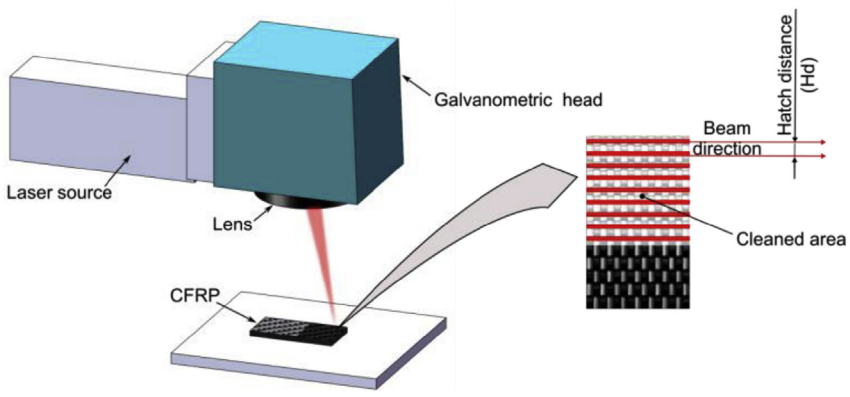


Fig. 1. Schematic of CFRP laser surface treatment.

Table 3
Control factors and levels of LAJ process.

Control factor	Level (−1)	Level (0)	Level (+1)
CFRP surface	As Received (AR)	–	Laser Cleaned (LC)
Laser power, P [W]	100	150	200
Linear energy, LE [J/mm]	3	4	5

based on preliminary tests and previous experiences [58], are reported in Table 3. The tests were conducted by varying: the CFRP surface condition (AR/LC), the laser power (P) and the linear energy (LE = P/Ss, were Ss is the scanning speed). It worth noting that the choice of the LE values was driven by the previous experience [58], where the maximum strength was reached for LE = 4.5 J/mm.

After the joining, single lap shear tests were carried out adopting a universal test machine, model 322.31 by MTS. The tests were conducted under quasi-static conditions (constant transverse speed of 0.5 mm/min). During the tests, the load and the displacement were recorded. Three replicates were performed for each testing condition; average and standard deviation of the Ultimate Tensile Force (UTF) and the apparent shear strength (τ_a) were determined. UTF was calculated as the maximum of the load measured during the test, while, τ_a was calculated as the ratio between the UTF and the joined area (which was measured after the test).

After the mechanical tests, a digital microscope (KH-8700 by Hirox), equipped with a 2.11 mega-pixel CCD sensor and motorized x-y table, was used to measure the adhesion area and to study the joint morphology.

Analysis of variance (ANOVA) was conducted to test the statistical significance of the process parameters on both the geometric and mechanical characteristics of the joints. The analysis was carried out at a 95% confidence level ($\alpha = 0.05$). ANOVA assumes that the observations are normally and independently distributed with the same variance for each treatment or factor level. Before the analysis, these assumptions were successfully checked via analysis of residuals. Moreover, the main effects plot and the interaction plot were adopted to analyse the effect of the process parameters.

In addition, to better understand the interaction phenomena occurring during the laser joining, the measure of the temperature reached on the laminate surface during the joining was carried out by Infrared thermography (IRT), adopting a IR-camera (model A655SC by FLIR), equipped with 24.5 mm lens.

As the PC is not transparent to the mean IR radiation (the camera has a spectral range of 7.5–14.0 μm), the thermal analysis was performed on the CFRP laminate without the PC sheet. This enabled to determine the temperature of the CFRP surface (as the poor thermal conductivity of the PC). Because of the great transmittance of the PC at the wavelength of $\lambda = 975$ nm (almost 90% [58,67]), the test were carried out at an equivalent laser power (P*) lowered by 10% with respect to that used during the LAJ tests. During the tests, the IR camera was placed at an angle of 60° with respect to the plane of the CFRP laminate and a distance of 250 mm. During the thermal analysis, shielding gas (N_2 at 2 bar) was adopted to avoid excessive formation of plasma.

3. Results

3.1. Morphological analysis of failure surfaces

Fig. 5 and Fig. 6 show the typical appearance of the PC surface after the single-lap shear tests for the as received (AR) and laser treated (LT) samples, respectively. For the AR samples (Fig. 5), the surfaces appearance is very similar to those reported in Ref. [58]. In particular, in the bonding area two different regions are visible: the first is placed at the centre of the irradiated area and a second one all around. The first region is characterized by the presence of fibre fragments coming from the CFRP laminates or by their imprint. In this area the CFRP is directly exposed to the laser radiation; the temperature reached by the fibres is so high to cause both the vaporization of the epoxy matrix and the PC softening. This produced an intimate contact between the softened polycarbonate and the heated fibres; thus, the bonding between the two materials is obtained.

The second region is characterized by the yellow surrounding area; in this region, the achieved temperature is not enough to produce the epoxy matrix vaporization because this area lies outside that directly irradiated by the laser beam. Thus, the heating occurs only by conduction. Moreover, due to the absence of direct contact between the fibres and the PC (as the presence of the epoxy resin layer that covers the carbon fibres), the temperature reached by the PC is lower than the first area. This leads to insufficient material softening. In this region, the vapours, produced by epoxy degradation and vaporization in the central zone, tend to flow sideways from the irradiated area and to condense. In these regions, the formation of an intimate contact between the PC and the laminate is even more difficult.

Similar remarks can be done in the case of laser cleaned surfaces (Fig. 6), even if the first area appears more regular along the scanning direction and an increase of the numbers of fibres attached to the PC is observable; this is due to the absence of epoxy matrix layer. Moreover, the yellowed area appears smaller in width and characterized by a comb shape. When the CFRP is cleaned from the superficial layer of epoxy, less vapour is produced during the laser joining as there is less amount of epoxy resin to vaporize; thus, initial cleaning has left voids between the weft and the warp from where the vapour can flow out.

The ANOVA was performed on the measured joined area width, to study the effect of the process parameters (P, LE, Treatment) on the bonding regions dimension. The result of the analysis is reported in Table 4. On the basis of assumptions made ($\alpha = 0.05$), all the process

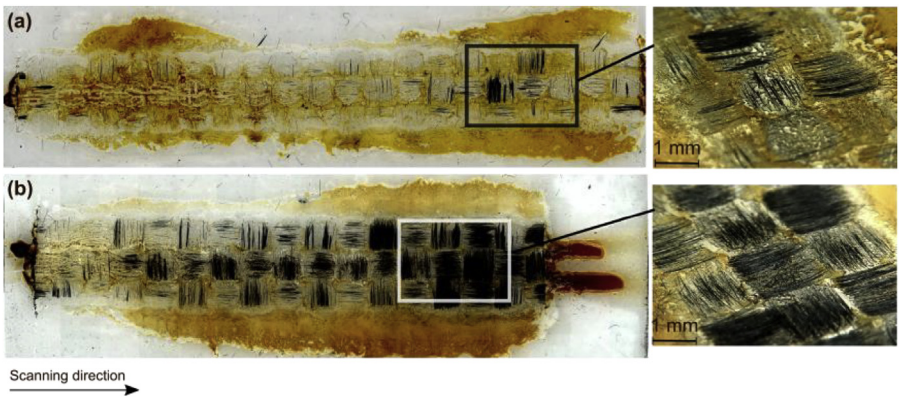


Fig. 5. Macrograph of PC after shear test, LE = 3 J/mm, CFRP Surface = AR: (a) P = 100 W, (b) P = 200 W.

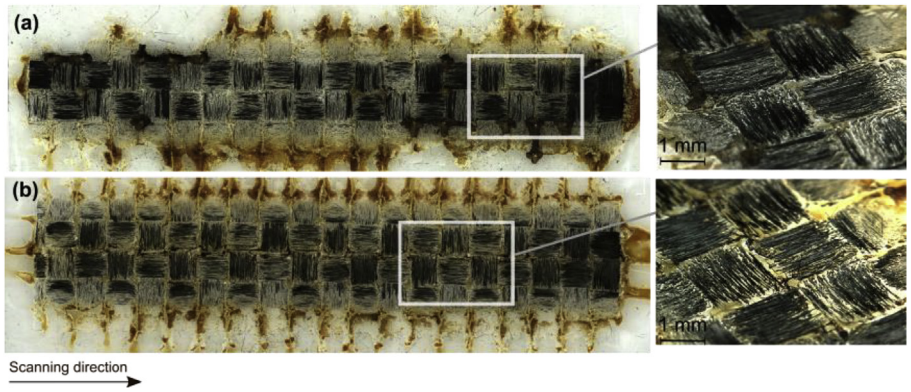


Fig. 6. Macrograph of PC after shear test, LE = 3 J/mm, CFRP Surface = LC and: (a) P = 100 W, (b) P = 200 W.

Table 4
ANOVA table for width.

Source	DF.	Seq. SS	Contrib. %	Adj, SS	Adj. MS	F-value	*p*-value
LE [J/mm]	2	4.779	3.13	4.779	2.389	8.57	**0.001**
Treatment	1	128.542	84.31	128.542	128.542	461.28	**0.000**
P [W]	2	2.865	1.88	2.865	1.433	5.14	**0.010**
LE*Treatment	2	2.041	1.34	2.041	1.020	3.66	**0.035**
LE*P	4	2.576	1.69	2.576	0.644	2.31	0.074
Treatments*P	2	0.521	0.34	0.521	0.261	0.94	0.401
Error	39	11.147	7.31	11.147	0.279		
Total	52	152.471	100.00				

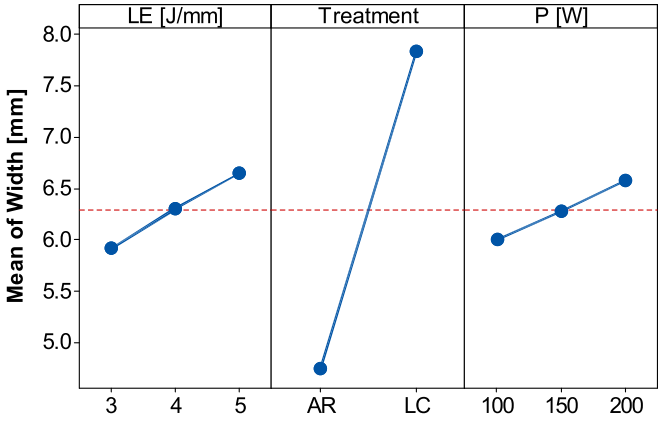


Fig. 7. Main effects plot for the width.

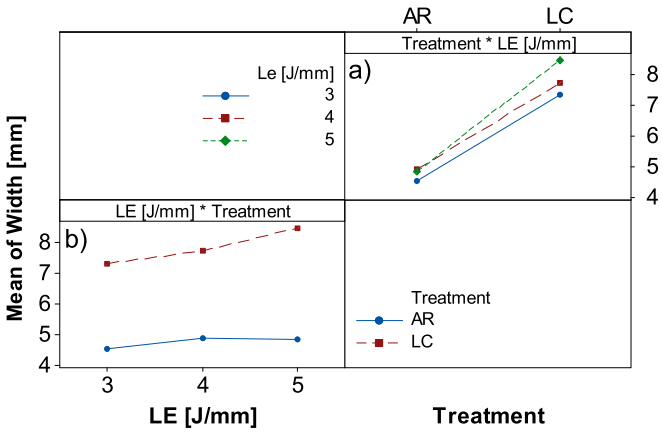


Fig. 8. Interaction plot for the width. Only significant interactions.

parameters are statistically significant (i.e the *p*-value is less than 0.05). Moreover, also the interaction between the linear energy and the surface treatment results significant.

In Fig. 7 and Fig. 8 the main effects plot and the interaction plot (only significant interactions) for the width are reported, respectively. From Fig. 7, as expected, the width increases at the increasing of the linear energy and the average power, or when the laser pre-treatment is adopted on the laminate (LC). The significant interaction (LE*Treatment) (shown in Fig. 8) reveals that on the untreated laminate (AR), the width remains almost constant at the LE changing. Conversely, when the laser cleaned laminate is adopted (LC), the increase of the width is more consistent (Fig. 7b).

3.2. Mechanical characterisation

The ANOVA results on ultimate tensile force and apparent shear strength results are summarized in Table 5 and Table 6. The results indicate that, the linear energy, the surface treatment and the interaction between the linear energy and the surface treatment are statistically significant for the UTF (Table 5). On the other hand, the apparent shear strength is affected only by the linear energy (Table 6).

In Fig. 9 and Fig. 10 the main effects plots for the ultimate tensile force (UTF) and the apparent shear strength (τ_a) are reported, respectively. In the plots, the significant parameters are highlighted using continuous lines. The figures show that, both UTF and τ_a decrease with increasing LE. In addition, the ultimate tensile force is much higher for treated (LC) as compared to as received (AR) condition.

Fig. 11 depicts the significant interaction (LE*Treatment) for the UTF. Similarly to what observed in the case of the width, the UTF of LC samples is more sensible to the linear energy changing as compared to the AR laminate (Fig. 11b).

3.3. Thermal analysis

Fig. 12 depicts the IR image of a CFRP specimen during laser irradiation, under P* = 200 W and LE = 5 J/mm. The IR maps show the

Table 5
ANOVA table for the ultimate tensile force (UTF).

Source	DF.	Seq. SS	Contrib. %	Adj, SS	Adj. MS	F-value	*p*-value
LE [J/mm]	2	0.83515	22.51	0.80534	0.40267	12.72	**0.000**
Treatment	1	1.06233	28.63	1.03587	1.03587	32.73	**0.000**
P [W]	2	0.03921	1.06	0.03240	0.01620	0.51	0.603
LE*Treatment	2	0.29649	7.99	0.29832	0.14916	4.71	**0.015**
LE*P	4	0.08308	2.24	0.07406	0.01852	0.58	0.675
Treatment*P	2	0.15934	4.29	0.15934	0.07967	2.52	0.090
Error	39	1.23447	33.27	1.23447	0.03165		
Total	52	3.71008	100.00				

Table 6
ANOVA table for the apparent shear strength (τ_a).

Source	DF	Seq. SS	Contrib. %	Adj, SS	Adj. MS	F-value	*p*-value
LE [J/mm]	2	18.8567	36.90	19.2779	9.6389	16.10	**0.000**
Treatment	1	0.1934	0.38	0.2336	0.2336	0.39	0.536
P [W]	2	0.4684	0.92	0.4210	0.2105	0.35	0.706
LE*Treatment	2	2.3082	4.52	2.3687	1.1844	1.98	0.152
LE*P	4	2.8273	5.53	2.6302	0.6575	1.10	0.371
Treatment*P	2	3.0987	6.06	3.0987	1.5493	2.59	0.088
Error	39	23.3545	45.70	23.3545	0.5988		
Total	52	51.1072	100.00				

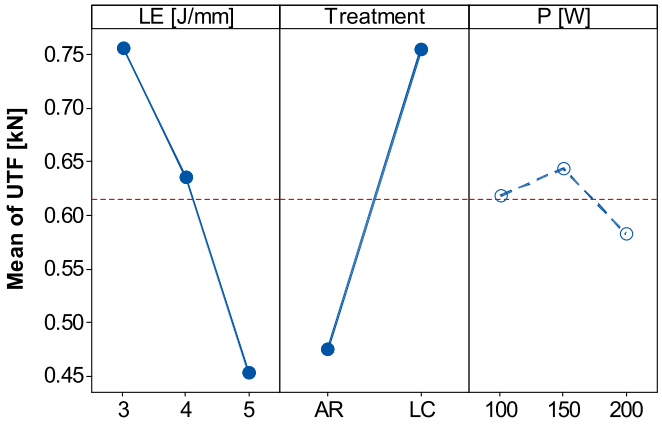


Fig. 9. Main effects plot for the ultimate tensile failure (UTF).

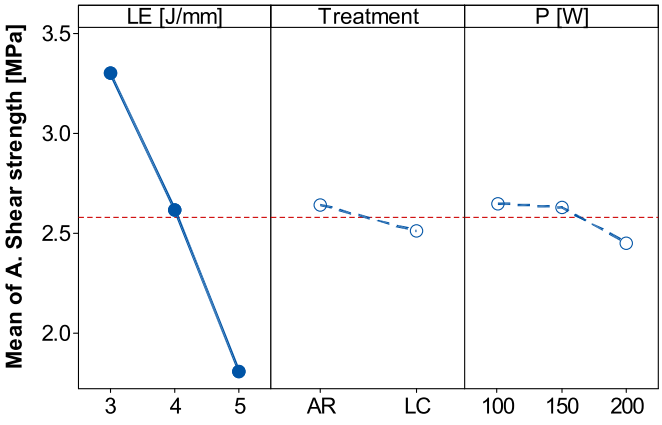


Fig. 10. Main effects plot for the apparent shear strength (τ_a).

presence of vapours, which are due to the degradation and vaporization of the epoxy matrix, covering the specimen even though the adoption of a shielding gas. These vapours exert a shield effect. Actually, they absorb the infrared radiation and prevent the correct absorption of the laser radiation as well as temperature measurement issues. Consequently, the thermal analysis is able to provide only qualitative and

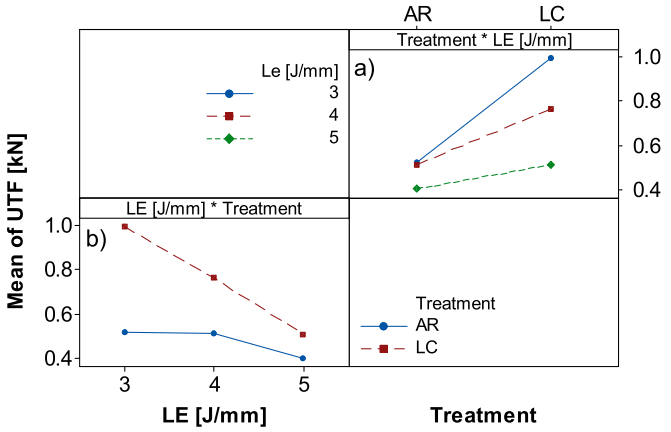


Fig. 11. Interaction plot for the ultimate tensile failure (UTF). Only significant interactions.

comparative information about LAJ performed on AR and LC samples. The maximum temperature versus the process time is reported in Fig. 13 and Fig. 14 for the different process conditions. In the figures, the curves are shifted for more clarity. The maximum temperature tends to increase with increasing LE; moreover, the temperature measured on LC samples was always higher than that observed on AR samples. Actually, when LAJ is performed on AR samples, part of the laser energy is spent to remove the epoxy resin on the laminate surface. This limited the temperature at the CFRP/PC interface.

Fig. 15 shows the acquired temperature in the transverse direction with respect to the joining one, just after the beam passing for LE = 5, P* = 100 W, and LE = 3, P* = 200 W. In the figure the dashed lines represent the melting (Tm) and the degradation (Td) temperatures of PC (230 °C and 540 °C, respectively). The figure clearly indicates for LC samples a slight enlargement of the areas where Tm and Td intersect the temperature profile. Similar results were obtained for the other combinations. However, these diagrams were not reported for sake of briefness.

4. Discussion

The influence of the process parameters on the width of the joint

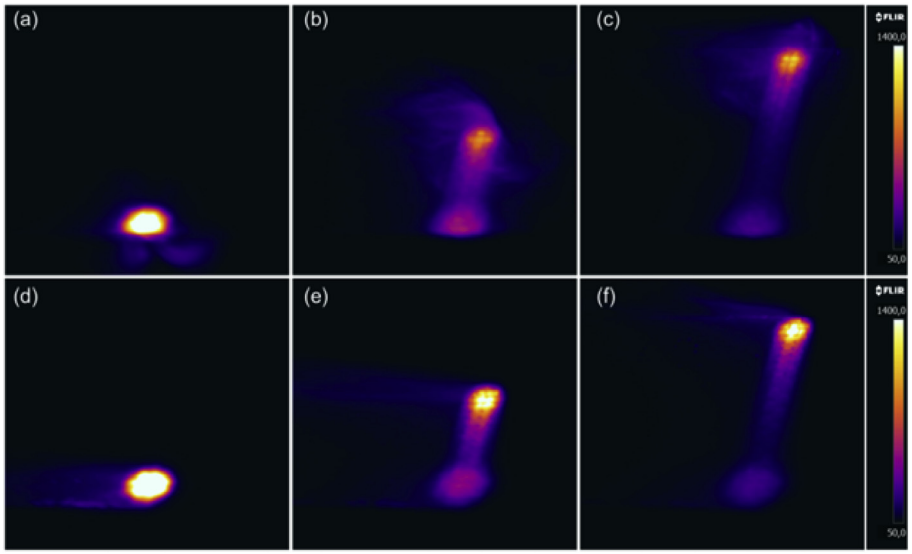


Fig. 12. IR image of CFRP laminate during laser irradiation for P* = 200 W and LE = 5 J at: a) inlet; b) centre; c) outlet of a AR sample; at d) inlet; e) centre; f) outlet of a LC sample.

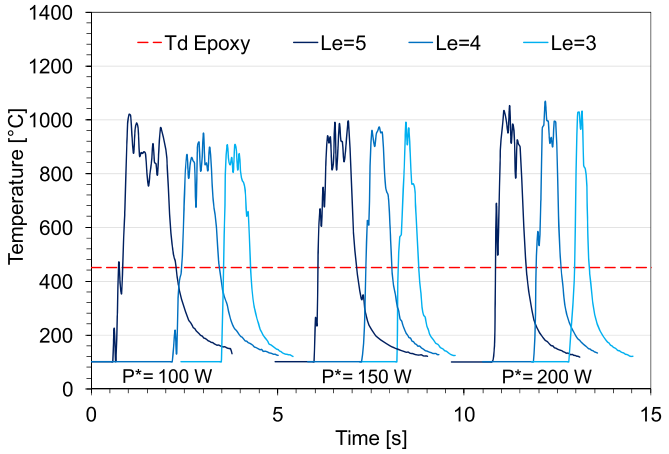


Fig. 13. Maximum temperature vs time for as received (AR) laminate.

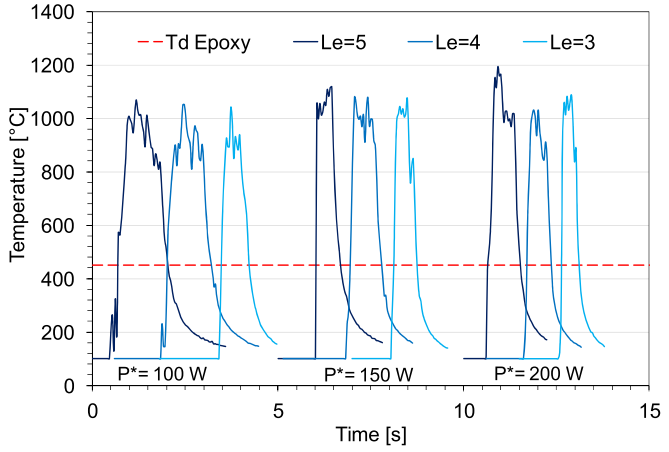


Fig. 14. Maximum temperature vs time for laser cleaned (LC) laminate.

region can be explained considering that: the increase of LE involves an increase of the energy released on the same surface. This comes with an increase of the maximum temperature and, consequently, an enlargement of the area where the same temperature is reached (Figs. 13 and 14).

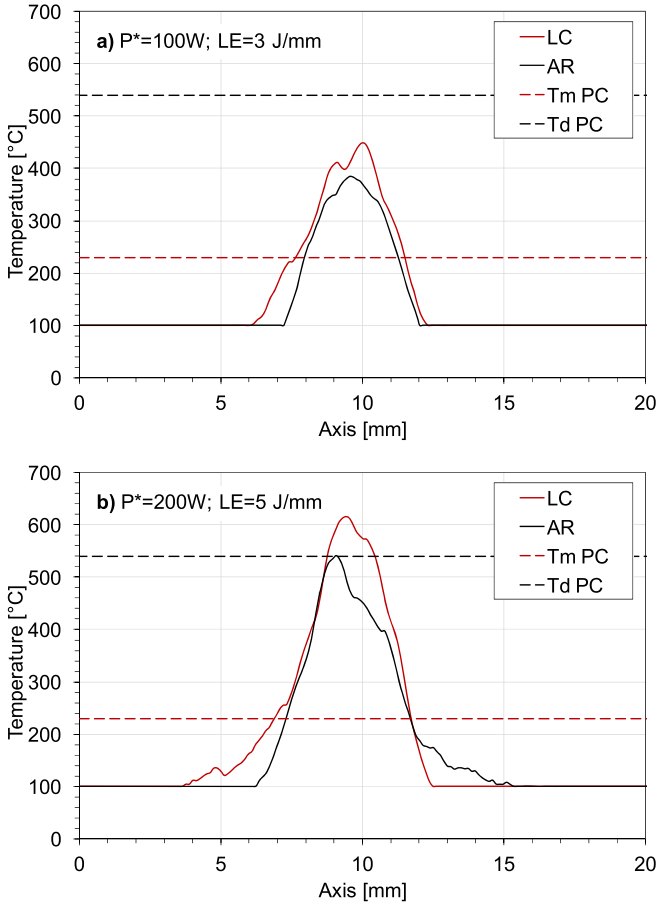


Fig. 15. Temperature profile as a function of x axis for: a) Le = 3 J/mm, P* = 100 W; b) LE = 5 J/mm, P* = 200 W.

The use of higher power levels involved the adoption of higher scan speeds (at the same LE) and, consequently, lower interaction times. Under these conditions, the heat has less time to diffuse into the inner layers and tends to be restricted on the surface of the CFRP. This results in a larger joined area (i.e. width) that exceeds the threshold temperature required for joining. It is worth noting that, not all the heated area concurs in the joining. In the central part (in correspondence of the

beam axis) PC degradation occurs while peripheral regions do not reach the PC melting temperature. These region have a marginal contribute to the strength of the joint.

The adoption of the laser cleaning involves a direct contact between the carbon fibres and the PC. This leads to a more efficient heating of the PC and to a better gas evacuation (as confirmed by the analysis of Fig. 6). Moreover, the part of the energy that was lost in the epoxy matrix degradation (i.e. vaporization) becomes available to heat the fibres. This also influences the joined area (i.e. the width) that is larger for LC samples.

The LE*Treatment interaction can be explained as the following: in the case of AR laminate, the laser radiation vaporizes only the portion of epoxy matrix directly exposed to the radiation. Consequently, in the surrounding area, the bonding is prevented by the resin layer that, independently from the temperature achieved, covers the carbon fibres. On the contrary, in the case of LC laminate, the absence of the first matrix layer facilitates the joining between the PC and the carbon fibres, making the joint width more sensitive to the increase of the linear energy.

However, the increase of the bonding area (i.e. width) does not necessarily involve an increase of UTF. Actually, UTF depends on several factors, including: the dimension of the adhesion area, the adhesion of the PC to the carbon fibres, the extension of the area where PC degradation occurs, as well as the laminate degradation.

The increase of the maximum temperature, due to increase of LE or P, produces a larger joined area and width where the degradation temperature of the PC rises (as showed in Fig. 15). Moreover, here, during the joining (i.e. the diode laser irradiation), the laminate undergoes a strong thermal stress. This over-heating may result in degradation/sublimation of the matrix placed under the exposed fibres, leading to formation of cavities, according to the observations reported in Refs. [63,65]. Thus, it is reasonable to suppose that a reduction in the load capability of the fibres, which detach from the underlying layers, may occur. This effect is higher when the laminate is cleaned (i.e. without the first matrix layer that covers the fibres), because of the highest temperature (Figs. 13–15). Thus, an increase of the linear energy or of the laser power, lead to the increase of both the apparent adhesion surface (i.e. width) and the degradation region, these aspects having adverse effects on the UTF. The increase in LE damages both the materials (laminate and PC) leading to a reduction of UTF. This reduction is partially compensated by the increase in the adhesion surface which occurs when the laminate is cleaned (LC). As a consequence, the laser cleaning treatment, promoting the increase in the adhesion area, results in an improvement in the UTF. Conversely, within the analysed processing window, considering the apparent shear strength, laser pretreatment does not produce a significant advantage.

From the process point of view, although the apparent shear strength does not increases when laser cleaning is adopted, from a practical point of view, the laser cleaning results in a reduction of the process time as the same joint resistance can be obtained by way of a single scanning line or highest scan speed.

5. Conclusions

Laser Assisted Joining Process (LAJ) between CFRP and PC sheet was investigated under different process conditions with and without laser cleaning pre-treatment of CFRP. Single lap joint test was performed to determine the quality of the joints. From the results, for the adopted laser sources and under the experimental conditions adopted here, the main conclusions are the following:

- laser cleaning process enables removing the first epoxy matrix layer from the laminate. This has great benefits on the joints morphology since the complete absence of degraded epoxy within the joined region, the easy removal of vapours due to the polymers degradation, as well as the increase of the joined area;
- under the adopted conditions, the temperatures reached on the CFRP during the joining, may arise the PC degradation temperature and produce damages on the CFRP laminate. Thus, in the centre of the bonded region a damaged area can be produced. This reduces the overall joint efficiency;
- although the increase of the linear energy involves an increase of the apparent bonded area (i.e. the joint width), for both the types of joined samples (AR and LC), the ultimate tensile failure load and the apparent shear strength decrease with the increasing of the linear energy;
- the average power does not result to be a statistically significant neither for UTS, neither for the apparent shear strength;
- in the industrial applications, the use of laser cleaning results in a reduction of the process time as the same joint resistance can be obtained by way of a single scanning line or highest scan speed.

Acknowledgements

The authors would like to thank Prof. Ko (Graduate School of Convergence Science, Pusan National University, Busan, 46241, South Korea) for supplying the CFRP samples. The authors would also like to thank Mr G. Organtini (DIIIE, University of L'Aquila) for his contribution during the setup and performance of the experimental tests. Finally, the authors would like to mention that the present work is a joint collaboration within Promozione L@aser, section of the Associazione Italiana Tecnologia Meccanica (AITeM).

References

[1] Tanaka K, Suzue M, Isshiki S, Shinohara M, Katayama T. Evaluation of the interfacial and interlaminar shear strength of carbon fiber reinforced polycarbonate made by a unidirectional sheet. 2014;1:291–9.
[2] Girão Coelho AM, Mottram JT. A review of the behaviour and analysis of bolted connections and joints in pultruded fibre reinforced polymers. Mater Des 2015;74:86–107.
[3] Lambiase F, Di Ilio A. Mechanical clinching of metal–polymer joints. J Mater Process Technol 2015;215:12–9.
[4] Lambiase F. Mechanical behaviour of polymer-metal hybrid joints produced by clinching using different tools. Mater Des 2015;87:606–18.
[5] Lee S-H, Lee C-J, Lee K-H, Lee J-M, Kim B-M, Ko D-C. Influence of tool shape on hole clinching for carbon fiber-reinforced plastic and SPRC440. Adv Mech Eng 2014;2014:1–12.
[6] Lee C-J, Lee J-M, Ryu H-Y, Lee K-H, Kim B-M, Ko D-C. Design of hole-clinching process for joining of dissimilar materials – Al6061-T4 alloy with DP780 steel, hot-pressed 22MnB5 steel, and carbon fiber reinforced plastic. J Mater Process Technol 2014;214:2169–78.
[7] Lambiase F, Ko D-C. Feasibility of mechanical clinching for joining aluminum AA6082-T6 and Carbon Fiber Reinforced Polymer sheets. Mater Des 2016;107:341–52.
[8] Lambiase F, Paoletti A. Friction-assisted clinching of Aluminum and CFRP sheets. J Manuf Process 2018;31:812–22.
[9] Lambiase F, Ko D-C. Two-steps clinching of aluminum and carbon fiber reinforced polymer sheets. Compos Struct 2017;164:180–8.
[10] Bouchikhi AS, Megueni A, Gouasmi S, Boukoulda FB. Effect of mixed adhesive joints and tapered plate on stresses in retrofitted beams bonded with a fiber-reinforced polymer plate. Mater Des 2013;50:893–904.
[11] Grewell D, Benatar A. Welding of plastics: fundamentals and new developments. Int Polym Process 2007;22:43–60.
[12] Mandolfino C, Lertora E, Genna S, Leone C, Gambaro C. Effect of laser and plasma surface cleaning on mechanical properties of adhesive bonded joints. Procedia CIRP 2015;33:458–63.
[13] Wang YY, Wang AH, Weng ZK, Xia HB. Laser transmission welding of Clearweld-coated polyethylene glycol terephthalate by incremental scanning technique. Optic Laser Technol 2016;80:153–61.
[14] Liu FC, Liao J, Nakata K. Joining of metal to plastic using friction lap welding. Mater Des 2014;54:236–44.
[15] Okada T, Uchida S, Nakata K. Direct joining of aluminum alloy and plastic sheets by friction lap processing. Mater Sci Forum 2014;794–796:395–400.
[16] Nagatsuka K, Yoshida S, Tsuchiya A, Nakata K. Direct joining of carbon-fiber–reinforced plastic to an aluminum alloy using friction lap joining. Compos B Eng 2015;73:82–8.
[17] Goushegir SM, dos Santos JF. Amancio-Filho ST. Friction Spot Joining of aluminum AA2024/carbon-fiber reinforced poly(phenylene sulfide) composite single lap joints: microstructure and mechanical performance. Mater Des 2014;54:196–206.
[18] Oliveira PHF, Amancio-Filho ST, dos Santos JF, Hage E. Preliminary study on the feasibility of friction spot welding in PMMA. Mater Lett 2010;64:2098–101.
[19] Junior WS, Emmler T, Abetz C, Handge UA, dos Santos JF, Amancio-Filho ST, et al.

Friction spot welding of PMMA with PMMA/silica and PMMA/silica-g-PMMA nanocomposites functionalized via ATRP. Polymer 2014;55:5146–59.
[20] Yusof F, Muhamad M, Moshwan R, Jamaludin M, Miyashita Y. Effect of surface states on joining mechanisms and mechanical properties of aluminum alloy (A5052) and polyethylene terephthalate (PET) by dissimilar friction spot welding. Metals 2016;6:101.
[21] Lambiase F, Paoletti A, Grossi V, Genna S. Improving energy efficiency in friction assisted joining of metals and polymers. J Mater Process Technol 2017;250:379–89.
[22] Goushegir SM, dos Santos JF, Amancio-Filho ST. Influence of process parameters on mechanical performance and bonding area of AA2024/carbon-fiber-reinforced poly (phenylene sulfide) friction spot single lap joints. Mater Des 2015;83:431–42.
[23] Gonçalves J, dos Santos JF, Canto LB, Amancio-Filho ST. Friction spot welding of carbon fiber-reinforced polyamide 66 laminate. Mater Lett 2015;159:506–9.
[24] Esteves JV, Goushegir SM, dos Santos JF, Canto LB, Hage E, Amancio-Filho ST. Friction spot joining of aluminum AA6181-T4 and carbon fiber-reinforced poly (phenylene sulfide): effects of process parameters on the microstructure and mechanical strength. Mater Des 2015;66:437–45.
[25] Junior WS, Handge UA, dos Santos JF, Abetz V, Amancio-Filho ST. Feasibility study of friction spot welding of dissimilar single-lap joint between poly(methyl methacrylate) and poly(methyl methacrylate)-SiO2 nanocomposite. Mater Des 2014;64:246–50.
[26] Amancio-Filho ST, Bueno C, dos Santos JF, Huber N, Hage E. On the feasibility of friction spot joining in magnesium/fiber-reinforced polymer composite hybrid structures. Materials Science and Engineering: A. 2011;528:3841–8.
[27] Katayama S, Kawahito Y. Laser direct joining of metal and plastic. Scripta Mater 2008;59:1247–50.
[28] Yousefpour A, Hojjati M, Immarigeon J-P. Fusion bonding/welding of thermoplastic composites. J Thermoplast Compos Mater 2004;17:303–41.
[29] Wippo V, Jaeschke P, Brueggmann M, Suttmann O, Overmeyer L. Advanced laser transmission welding strategies for fibre reinforced thermoplastics. Phys Procedia 2014;56:1191–7.
[30] Aden M. Influence of the laser-beam distribution on the seam dimensions for laser-transmission welding: a simulative approach. Lasers Manufact Mater Process 2016;3:100–10.
[31] Sooriyapiragasam SK, Hopmann C. Modeling of the heating process during the laser transmission welding of thermoplastics and calculation of the resulting stress distribution. Weld World 2016;60:777–91.
[32] Hadriche I, Ghorbel E, Masmoudi N, Casalino G. Investigation on the effects of laser power and scanning speed on polypropylene diode transmission welds. Int J Adv Manuf Technol 2010;50:217–26.
[33] Ghorbel E, Casalino G, Abed S. Laser diode transmission welding of polypropylene: geometrical and microstructure characterisation of weld. Mater Des 2009;30:2745–51.
[34] Xu XF, Parkinson A, Bates PJ, Zak G. Effect of part thickness, glass fiber and crystallinity on light scattering during laser transmission welding of thermoplastics. Optic Laser Technol 2015;75:123–31.
[35] Xu XF, Bates PJ, Zak G. Effect of glass fiber and crystallinity on light transmission during laser transmission welding of thermoplastics. Optic Laser Technol 2015;69:133–9.
[36] Liu H, Chen G, Jiang H, Guo D, Yan Z, Wu X, et al. Performance and mechanism of laser transmission joining between glass fiber-reinforced PA66 and PC. J Appl Polym Sci 2016;133:1–8.
[37] Asséko ACA, Cosson B, Schmidt F, Maoult YL, Lafranche E. Laser transmission welding of composites-Part A: thermo-physical and optical characterization of materials. Infrared Phys Technol 2015;72:293–9.
[38] Jaeschke P, Wippo V, Suttmann O, Overmeyer L. Advanced laser welding of high-performance thermoplastic composites. J Laser Appl 2015;27:S29004.
[39] Acherjee B, Kuar AS, Mitra S, Misra D. Empirical modeling and multi-response optimization of laser transmission welding of polycarbonate to ABS. Lasers Manufact Mater Process 2015;2:103–23.
[40] Bates PJ, Okoro TB, Chen M. Thermal degradation of PC and PA6 during laser transmission welding. Weld World 2014;59:381–90.
[41] Wang X, Zhang C, Li P, Wang K, Hu Y, Zhang P, et al. Modeling and optimization of joint quality for laser transmission joint of thermoplastic using an artificial neural network and a genetic algorithm. Optic Laser Eng 2012;50:1522–32.
[42] Chen M, Zak G, Bates PJ. Description of transmitted energy during laser transmission welding of polymers. Weld World 2012;57:171–8.
[43] Acherjee B, Kuar AS, Mitra S, Misra D, Acharyya S. Experimental investigation on laser transmission welding of PMMA to ABS via response surface modeling. Optic Laser Technol 2012;44:1372–83.
[44] Jung K-W, Kawahito Y, Katayama S. Mechanical property and joining characteristics of laser direct joining of CFRP to polyethylene terephthalate. Int J Precis Eng Manuf-Green Technol 2014;1:43–8.
[45] Jung KW, Kawahito Y, Takahashi M, Katayama S. Laser direct joining of carbon fiber reinforced plastic to zinc-coated steel. Mater Des 2013;47:179–88.
[46] Jung KW, Kawahito Y, Katayama S. Laser direct joining of CFRP to metal or engineering plastic. Trans JWRI 2013;42.
[47] Wang X, Chen H, Liu H, Li P, Yan Z, Huang C, et al. Simulation and optimization of continuous laser transmission welding between PET and titanium through FEM, RSM, GA and experiments. Optic Laser Eng 2013;51:1245–54.
[48] Liu H, Wang K, Li P, Zhang C, Du D, Hu Y, et al. Modeling and prediction of transmission laser bonding process between titanium coated glass and PET based on response surface methodology. Optic Laser Eng 2012;50:440–8.
[49] Wang X, Li P, Xu Z, Song X, Liu H. Laser transmission joint between PET and titanium for biomedical application. J Mater Process Technol 2010;210:1767–71.
[50] Chan C-W, Smith GC. Fibre laser joining of highly dissimilar materials: commercially pure Ti and PET hybrid joint for medical device applications. Mater Des 2016;103:278–92.
[51] Chen YJ, Yue TM, Guo ZN. A new laser joining technology for direct-bonding of metals and plastics. Mater Des 2016;110:775–81.
[52] Hussein FI, Akman E, Genc Oztoprak B, Gunes M, Gundogdu O, Kacar E, et al. Evaluation of PMMA joining to stainless steel 304 using pulsed Nd:YAG laser. Optic Laser Technol 2013;49:143–52.
[53] Hussein FI, Salloomi KN, Akman E, Hajim KI, Demir A. Finite element thermal analysis for PMMA/st.st.304 laser direct joining. Optic Laser Technol 2017;87:64–71.
[54] Georgiev GL, Baird RJ, McCullen EF, Newaz G, Auner G, Patwa R, et al. Chemical bond formation during laser bonding of Teflon® FEP and titanium. Appl Surf Sci 2009;255:7078–83.
[55] Yusof F, Yukio M, Yoshiharu M, Abdul Shukor MH. Effect of anodizing on pulsed Nd:YAG laser joining of polyethylene terephthalate (PET) and aluminium alloy (A5052). Mater Des 2012;37:410–5.
[56] Jung D-J, Cheon J, Na S-J. Effect of surface pre-oxidation on laser assisted joining of acrylonitrile butadiene styrene (ABS) and zinc-coated steel. Mater Des 2016;99:1–9.
[57] Lambiase F, Genna S, Kant R. A procedure for calibration and validation of FE modelling of laser-assisted metal to polymer direct joining. Optic Laser Technol 2018;98:363–72.
[58] Lambiase F, Genna S, Leone C, Paoletti A. Laser-assisted direct-joining of carbon fibre reinforced plastic with thermosetting matrix to polycarbonate sheets. Optic Laser Technol 2017;94:45–58.
[59] Lambiase F, Paoletti A, Di Ilio A. Effect of tool geometry on loads developing in friction stir spot welds of polycarbonate sheets. Int J Adv Manuf Technol 2016;87:2293–303.
[60] Jang BN, Wilkie CA. The thermal degradation of bisphenol A polycarbonate in air. Thermochim Acta 2005;426:73–84.
[61] Ahamad T, Alshehri SM. Thermal degradation and evolved gas analysis of epoxy (DGEBA)/novolac resin blends (ENB) during pyrolysis and combustion. J Therm Anal Calorim 2012;111:445–51.
[62] Leone C, Papa I, Tagliaferri F, Lopresto V. Investigation of CFRP laser milling using a 30W Q-switched Yb:YAG fiber laser: effect of process parameters on removal mechanisms and HAZ formation. Compos Appl Sci Manuf 2013;55:129–42.
[63] Fischer F, Kreling S, Jäschke P, Frauenhofer M, Kracht D, Dilger K. Laser surface pre-treatment of CFRP for adhesive bonding in consideration of the absorption behaviour. J Adhes 2012;88:350–63.
[64] Genna S, Leone C, Ucciardello N, Giuliani M. Increasing adhesive bonding of carbon fiber reinforced thermoplastic matrix by laser surface treatment. Polym Eng Sci 2017;57:685–92.
[65] Völkermeyer F, Jaeschke P, Stute U, Kracht D. Laser-based modification of wettablility for carbon fiber reinforced plastics. Appl Phys A 2012;112:179–83.
[66] Lambiase F, Genna S. Laser-assisted direct joining of AISI304 stainless steel with polycarbonate sheets: thermal analysis, mechanical characterization, and bonds morphology. Optic Laser Technol 2017;88:205–14.
[67] Ghorbel E, Hadriche I, Casalino G, Masmoudi N. Characterization of thermo-mechanical and fracture behaviors of thermoplastic polymers. Materials (Basel) 2014;7:375–98.